

Mobility matrix of a weakly coupled parallel multi-DIM isolator based on axial force solution^①

Li Desheng(李德胜), Yu Jiangtao, Huang Baowang, Li Zhanxian, Wang Zhijun^②

(College of Mechanical Engineering, North China University of Science and Technology, Tangshan 063210, P. R. China)

Abstract

A mobility matrix modeling strategy based on axial force solution for a weakly coupled parallel multi-dimensional (multi-DIM) isolator is proposed. Mobility power flow and transmissibility through the isolator are derived from the mobility matrix. Comparison between simulation and experimental results shows the correctness of the proposed modeling strategy.

Key words: mobility matrix, weak-coupling, parallel multi-dimensional (multi-DIM) isolator, axial force, mobility power flow

0 Introduction

Parallel multi-dimensional (multi-DIM) isolator is a special kind of vibration isolator, which can be decomposed into two end-platforms and the isolation limbs. Parallel multi-DIM isolator may be used in some application fields where traditional isolator cannot be used due to limitation of the complexity of vibration, especially when the vibration occurs in several dimensions simultaneously. This characteristics has attracted the interest of many researchers^[1,2].

A parallel mechanism is designed in such a way that all the components including the outer framework are subjected only to tensile-compressive forces, but not to flexing, thus eliminating the need for any special machine foundation. In other words, this rigid, self-contained structure enables its capabilities to be independent of the qualities of its foundation so that it can be mounted on a movable platform.

Thanks to these structural properties, Stewart platform has gained more popularity in multi-DIM vibration isolation applications^[3-8]. Hanieh^[9] investigated the application of the Stewart platform with flexible joints in the active vibration isolation and damping of the sensitive equipment. Each leg of her Stewart platform consisted of a voice coil actuator, a force sensor and two flexible joints. In the field of large amplitude vibration control, Cheng et al.^[10] and Ren et al.^[11] studied the vibration control of the Stewart platform on flexibly supported structures. Their work was further

developed by Lu et al.^[12] later, and the field model experiments manifested the effectiveness of the Stewart platform in isolating the vibration and improving the positioning and orientating accuracy.

Apart from the Stewart platform, parallel mechanism with lower-mobility is also often used in multi-DIM vibration control. In Refs[13,14], a 3-axis active vibration isolation system with pneumatic actuators using modified zero-power control was developed. In Ref. [15], a 3-PUPU dual parallel manipulator for both rough positioning and active vibration isolation in a wide-range workspace was presented. In Ref. [16], the dynamic modeling and efficient modal control of a planar parallel manipulator with 3 flexible linkages actuated by linear ultrasonic motors was addressed.

However, strong-coupling always makes the practical isolation performance not up to expectations, especially for higher-mobility cases^[17]. In view of this, a mobility matrix modeling strategy of a weakly coupled parallel multi-DIM isolator based on axial force solution is proposed. Numerical simulations are given to prove the validity of the established mathematical model via mobility power flow method. Experimental results are also given to demonstrate the isolation performance.

This paper is structured into following sections: axial force solution of limbs is solved by means of Screw theory in Section 1. Then, mobility matrix of weakly coupled parallel multi-DIM isolator are investigated based on the axial force solution in Section 2. In Section 3, the total mobility power flow together with response on flexible foundation, including velocity and

① Supported by the National Natural Science Foundation of China (No. 51505124) and the Scientific Research Initiation Foundation of North China University of Science and Technology (No. 28405699).

② To whom correspondence should be addressed. E-mail: zjwang@ncst.edu.cn

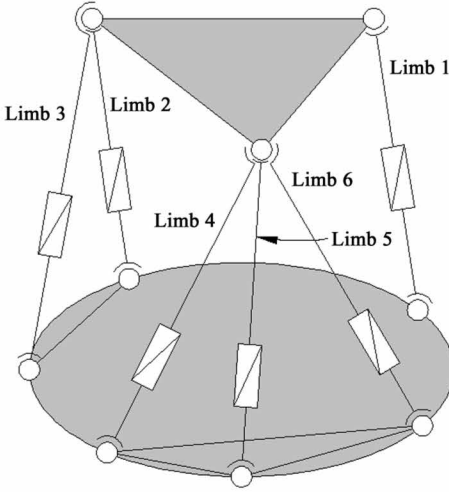
Received on Dec. 2, 2019

force at bottom spherical joints is simulated. Section 4 presents a multi-DIM vibrational experiment to validate the modeling strategy for mobility matrix and the mobility power flow.

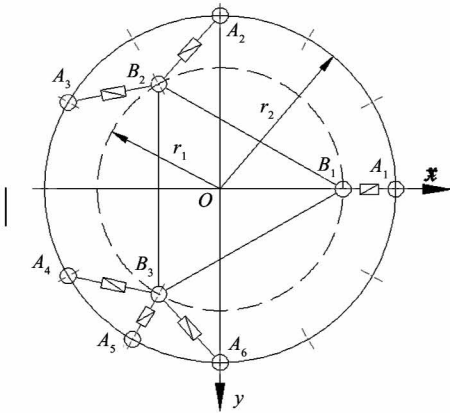
1 Axial force of weakly coupled parallel multi-DIM isolator

1.1 Structure description

The titled multi-DIM isolator can be obtained by adding spring and damping elements to 6 limbs of the ontology as shown in Fig. 1(a). Spherical joints B_1 - B_3 are distributed uniformly in a circle whose radius is r_1 , spherical joints A_1 - A_6 in a circle whose radius is r_2 . Top view with coordinate system o - xyz , in which z -axis assuming the same direction as gravity, is shown in Fig. 1(b). The damping performance is simulated in Ref. [18].



(a) Ontology of the isolator



(b) Sign convention and coordinates systems

Fig. 1 Weakly coupled parallel multi-DIM isolator

1.2 Axial force solution

Axial forces of 6 limbs can be expressed by force spinor. Considering balance of up platform, sum of 6 force spinors should be equal to 6-dimension forces acting on up platform. So the spiral equation can be written as

$$\sum_{i=1}^6 f_i \mathcal{S}_i = \mathbf{F} + \in \mathbf{M} \quad (1)$$

$$\mathcal{S}_i = \mathbf{S}_i + \in \mathbf{S}_{0i} \quad (2)$$

$$\mathbf{S}_i \cdot \mathbf{S}_i = 1 \quad (3)$$

$$\mathbf{S}_i \cdot \mathbf{S}_{0i} = 0 \quad (4)$$

where, f_i is axial force of the i -th limb. \mathcal{S}_i is identity linear vector of the i -th limb's axial line. \mathbf{F} and \mathbf{M} are vectors of principal exciting forces and moments, respectively, acting on up platform. \mathbf{S}_i is identity vector along the i -th limb, \mathbf{S}_{0i} is line moment of vector \mathbf{S}_i relative to the origin of coordinate system. Balance of spiral equation can be expressed in matrix form

$$\mathbf{F} = [\mathbf{G}_f^F] \mathbf{f} \quad (5)$$

where, $[\mathbf{G}_f^F]$ is the 1-st order static influence coefficient matrix of axial force \mathbf{f} on principal exciting force vector \mathbf{F} acting on up platform.

$$\mathbf{F} = [F_x \ F_y \ F_z \ M_x \ M_y \ M_z]^T \quad (6)$$

$$[\mathbf{G}_f^F] = \begin{bmatrix} S_1 & S_2 & \cdots & S_6 \\ S_{01} & S_{02} & \cdots & S_{06} \end{bmatrix} \quad (7)$$

$$\mathbf{f} = [f_1 \ f_2 \ \cdots \ f_6]^T \quad (8)$$

$$\mathbf{S}_i = \begin{cases} (B_1 - A_i) / |B_1 - A_i| & i = 1 \\ (B_2 - A_i) / |B_2 - A_i| & i = 2, 3 \\ (B_3 - A_i) / |B_3 - A_i| & i = 4, 5, 6 \end{cases} \quad (9)$$

$$\mathbf{S}_{0i} = \mathbf{A}_i \times \mathbf{S}_i \quad (10)$$

Inverse solution of Eq. (6) – Eq. (8) denotes axial forces, which can be solved as

$$\mathbf{f} = [\mathbf{G}_f^F]^{-1} \mathbf{F} \quad (11)$$

2 Mobility matrix modeling

2.1 Mobility matrix of rigid body source

The first substructure is rigid body source mounting at up platform, which can be regarded as a cylinder with radius r_A and center height h_A . It is assumed that the generalized exciting force acting at rigid body center, force vector \mathbf{F}_S and response velocity vector \mathbf{v}_S can be denoted as

$$\mathbf{F}_S = [F_x, F_y, F_z, M_x, M_y, M_z]^T \quad (12)$$

$$\mathbf{v}_S = [v_x, v_y, v_z, w_x, w_y, w_z]^T \quad (13)$$

Force and velocity response vectors at up spherical joints in coordinate system o - xyz could be marked as

$$\tilde{\mathbf{F}}_A = [\tilde{\mathbf{F}}_A^1, \tilde{\mathbf{F}}_A^2, \tilde{\mathbf{F}}_A^3]^T \quad (14)$$

$$\tilde{\mathbf{v}}_A = [\tilde{v}_A^1, \tilde{v}_A^2, \tilde{v}_A^3]^T \quad (15)$$

$$\tilde{\mathbf{F}}_A^i = [\tilde{\mathbf{F}}_{Ax}^i, \tilde{\mathbf{F}}_{Ay}^i, \tilde{\mathbf{F}}_{Az}^i, \tilde{\mathbf{M}}_{Ax}^i, \tilde{\mathbf{M}}_{Ay}^i, \tilde{\mathbf{M}}_{Az}^i]^T \quad (16)$$

$$\tilde{\mathbf{v}}_A^i = [\tilde{\mathbf{v}}_{Ax}^i, \tilde{\mathbf{v}}_{Ay}^i, \tilde{\mathbf{v}}_{Az}^i, \tilde{\boldsymbol{\omega}}_{Ax}^i, \tilde{\boldsymbol{\omega}}_{Ay}^i, \tilde{\boldsymbol{\omega}}_{Az}^i]^T \quad (17)$$

For convenience, local coordinate system O - UVP is created at up end of limb, whose origin is located at the spherical joint center. Axes of the local coordinate system are coincident with or perpendicular to limb when the isolator is in continuous motion state, as shown in Fig. 2.

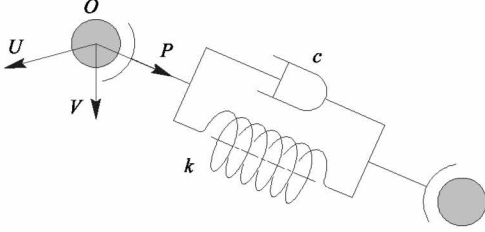


Fig. 2 Local coordinate system created at up end of limb

Output force and velocity vectors, \mathbf{F}_A and \mathbf{v}_A , at 3 up spherical joints, in local coordinate system, can be obtained from vectors $\tilde{\mathbf{F}}_A$ and $\tilde{\mathbf{v}}_A$ through coordinate transformation.

$$\mathbf{F}_A = [\mathbf{F}_A^1, \mathbf{F}_A^2, \dots, \mathbf{F}_A^6]^T \quad (18)$$

$$\mathbf{v}_A = [\mathbf{v}_A^1, \mathbf{v}_A^2, \dots, \mathbf{v}_A^6]^T \quad (19)$$

$$\mathbf{F}_A^i = [\mathbf{F}_{AU}^i, \mathbf{F}_{AV}^i, \mathbf{F}_{AP}^i, \mathbf{M}_{AU}^i, \mathbf{M}_{AV}^i, \mathbf{M}_{AP}^i]^T \quad (20)$$

$$\mathbf{v}_A^i = [\mathbf{v}_{AU}^i, \mathbf{v}_{AV}^i, \mathbf{v}_{AP}^i, \boldsymbol{\omega}_{AU}^i, \boldsymbol{\omega}_{AV}^i, \boldsymbol{\omega}_{AP}^i]^T \quad (21)$$

Mobility matrix equation of rigid body source can be determined according to rigid body dynamics theory

$$\begin{bmatrix} \mathbf{v}_s \\ \mathbf{v}_A \end{bmatrix} = \boldsymbol{\alpha} \begin{bmatrix} \mathbf{F}_s \\ \mathbf{F}_A \end{bmatrix} \quad (22)$$

where, $\boldsymbol{\alpha}$ is mobility matrix of the rigid body source.

2.2 Mobility matrix of absorber limb

The second substructure is absorber limb. The moments appearing in spherical joints could be transformed into general forces because torque couldn't be transferred through the rotational degree of freedoms (DOFs). Therefore, an absorber limb consisting of spring and damping mounted in parallel can be regarded as completely rigid in lateral, and could be molded as a complex stiffness spring. Considering the continuity of velocity and the equilibrium of force at the interface between two adjacent substructures, input variables of absorber limb must be equal to the output variables of rigid body source. Both ends of the absorber limb could be defined as input and output terminals represented by superscripts (1) and (2), respectively. Input force and velocity vectors at up end (1) in local coordinate system can be expressed as

$$\mathbf{F}_B^{(1)} = [\mathbf{F}_{B1}^{(1)}, \mathbf{F}_{B2}^{(1)}, \dots, \mathbf{F}_{B6}^{(1)}]^T \quad (23)$$

$$\mathbf{v}_B^{(1)} = [\mathbf{v}_{B1}^{(1)}, \mathbf{v}_{B2}^{(1)}, \dots, \mathbf{v}_{B6}^{(1)}]^T \quad (24)$$

$$\mathbf{F}_{Bi}^{(1)} = [\mathbf{F}_{Bui}^{(1)}, \mathbf{F}_{Bvi}^{(1)}, \mathbf{F}_{Bpi}^{(1)}, \mathbf{M}_{Bui}^{(1)}, \mathbf{M}_{Bvi}^{(1)}, \mathbf{M}_{Bpi}^{(1)}]^T \quad (25)$$

$$\mathbf{v}_{Bi}^{(1)} = [\mathbf{v}_{Bui}^{(1)}, \mathbf{v}_{Bvi}^{(1)}, \mathbf{v}_{Bpi}^{(1)}, \boldsymbol{\omega}_{Bui}^{(1)}, \boldsymbol{\omega}_{Bvi}^{(1)}, \boldsymbol{\omega}_{Bpi}^{(1)}]^T \quad (26)$$

Mobility matrix equation of absorber limb can be rearranged as

$$\begin{bmatrix} \mathbf{v}_B^{(1)} \\ \mathbf{v}_B^{(2)} \end{bmatrix} = \boldsymbol{\beta} \begin{bmatrix} \mathbf{F}_B^{(1)} \\ \mathbf{F}_B^{(2)} \end{bmatrix} \quad (27)$$

where, $\boldsymbol{\beta}$ is mobility matrix of absorber substructure.

2.3 Mobility matrix of flexible foundation

The third substructure is the flexible foundation, which could be molded as a clamped thin circular plate with concentrated masses at bottom spherical joints to simulate the pre-stressed effect of rigid body source under stationary and initial state. Combining 6 bottom spherical points into a module, mobility equation of flexible foundation can be described as

$$\mathbf{v}_C = \boldsymbol{\gamma} \mathbf{F}_C \quad (28)$$

where, $\boldsymbol{\gamma}$ is driving force mobility matrix of the flexible foundation, which can be deduced from modal analysis^[19,20].

2.4 Mobility matrix of the multi-DIM isolator

For the titled isolator, the continuity conditions of force and velocity must be satisfied. It means that the force and the velocity at interface between any 2 adjacent substructures could be described as

$$\mathbf{F}_A = -\mathbf{F}_B^{(1)}, \mathbf{v}_A = \mathbf{v}_B^{(1)} \quad (29)$$

$$\mathbf{F}_B^{(2)} = -\mathbf{F}_C \quad (30)$$

$$\mathbf{v}_B^{(2)} = \mathbf{v}_C \quad (31)$$

Mobility matrix equation of the whole isolator can be deduced by sequential multiplications of Eqs(22), (27) and (28). Velocity response vector \mathbf{v}_s at rigid body center, velocity and force response vectors \mathbf{v}_C and \mathbf{F}_C at 6 bottom spherical joints on flexible foundation could be obtained by recombining 3 mobility matrix equations

$$\mathbf{v}_s = (\boldsymbol{\alpha}_{11} + \boldsymbol{\alpha}_{12}\boldsymbol{\Theta})\mathbf{F}_s \quad (32)$$

$$\mathbf{v}_C = -\boldsymbol{\gamma}\boldsymbol{\Xi}\boldsymbol{\Theta}\mathbf{F}_s \quad (33)$$

$$\mathbf{F}_C = -\boldsymbol{\Xi}\boldsymbol{\Theta}\mathbf{F}_s \quad (34)$$

$$\boldsymbol{\Xi} = (\boldsymbol{\beta}_{22} + \boldsymbol{\gamma})^{-1}\boldsymbol{\beta}_{21} \quad (35)$$

$$\boldsymbol{\Theta} = (\boldsymbol{\beta}_{12}\boldsymbol{\Xi} - \boldsymbol{\alpha}_{22} - \boldsymbol{\beta}_{11})^{-1}\boldsymbol{\alpha}_{21} \quad (36)$$

The mobility matrix of multi-DIM isolator can be written as $\boldsymbol{\Gamma}$ in following equation

$$\begin{bmatrix} \mathbf{v}_s \\ \mathbf{v}_C \end{bmatrix} = \boldsymbol{\Gamma} \begin{bmatrix} \mathbf{F}_s \\ \mathbf{F}_C \end{bmatrix} \quad (37)$$

Mobility power flows into rigid body source and flexible foundation could be calculated as

$$P_{in} = 0.5\text{Re}[\mathbf{F}_s^H \cdot \mathbf{v}_s] \quad (38)$$

$$P_{out} = 0.5\text{Re}[\mathbf{F}_C^H \cdot \mathbf{v}_C] \quad (39)$$

where, superscript H represents Hermitian transpose

and conjugate of vector or matrix.

3 Numerical simulation and analysis

Assume amplitudes vector of the generalized excit-

ing force acting at mass center of rigid body source is $[1, 0, 1, 0, 1, 0]^T$ and the exciting frequency is 120 Hz. Geometric and material parameters of the isolator are given in Table 1.

Table 1 Geometric and material parameters of the multi-DIM isolator

| Substructure | Parameter | Unit | Value |
|--------------|------------------|----------------------------------|--|
| Rigid body | Radius | m | 0.135 |
| | Height | m | 0.178 |
| | Density | $\text{kg} \cdot \text{m}^{-3}$ | 7.850E03 |
| Foundation | Radius | m | 0.320 |
| | Thickness | m | 0.003 |
| | Density | $\text{kg} \cdot \text{m}^{-3}$ | 7.850E03 |
| | Young's modulus | MPa | 6.500E10 |
| | Poisson's ratio | — | 0.330 |
| | Loss factor | — | 0.020 |
| Absorber | Initial length | m | $l_1 = l_5 = 0.382, l_2 = l_3 = l_4 = l_6 = 0.440$ |
| | Spring stiffness | $\text{N} \cdot \text{m}^{-1}$ | $k_1 = 2k_2 = 2k_3 = 3k_4 = 3k_5 = 3k_6 = 3\,000$ |
| | Damping value | $\text{N s} \cdot \text{m}^{-1}$ | $c_1 = 2c_2 = 2c_3 = 3c_4 = 3c_5 = 3c_6 = 450$ |

Driving point mobility matrix of the flexible foundation can be obtained according to Ref. [1]. Transverse velocity and force responses at bottom spherical joints can be solved as shown in Fig.3 and Fig.4.

It can be observed from Fig.3 and Fig.4 that transverse velocity and force responses are ellipse in complex plane, which suggests that velocity and force response at bottom spherical joints are periodically fluctuant and the amplitude approximates to a constant. However, for the response at spherical joint A_1 , the ellipses of velocity and force in complex plane, show as an obvious distortion. The reason is that limb 1 is a single opened chain with more difficulty of decoupling. The spherical joints A_2 - A_6 belong to limbs 2 – 6 with one or two loops, which makes the hybrid single opened chain with less difficulty of decoupling.

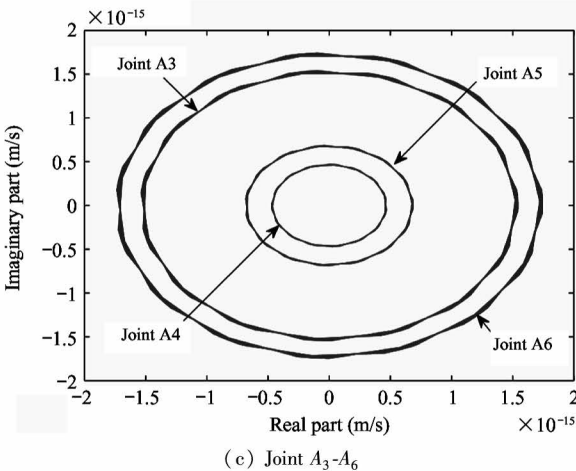
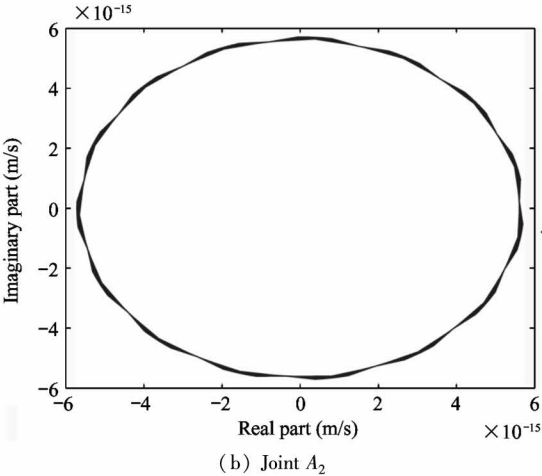
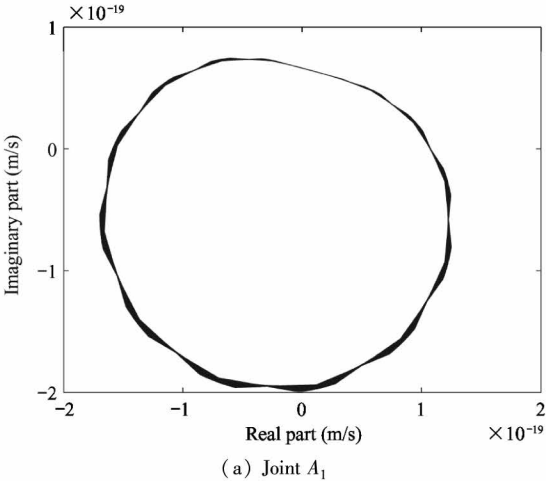


Fig. 3 Transverse velocity response at bottom spherical joints in complex plane

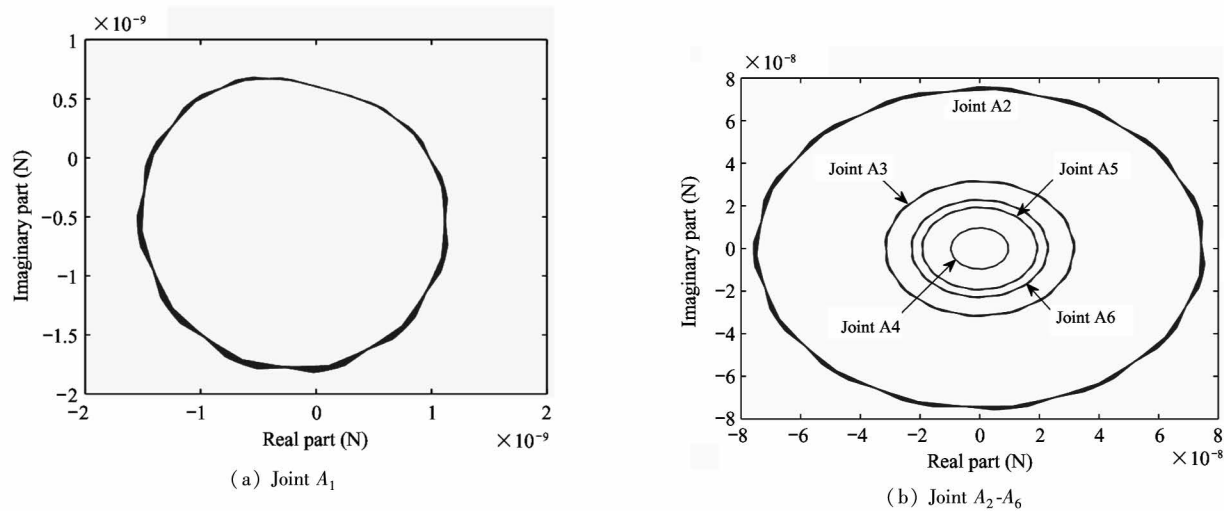


Fig. 4 Transverse force response at bottom spherical joints in complex plane

Fig. 5 shows axial forces of 6 limbs. It can be seen from the plots that periodicity of axial force is constant with the exciting force because the ellipse outline fluctuates smoothly. However, the axial force is not

simply harmonic due to the ellipse is inclined. Numerical migration between geometry center and origin suggests that the amplitude of axial force is not a constant and axial force is nonzero at balance position.

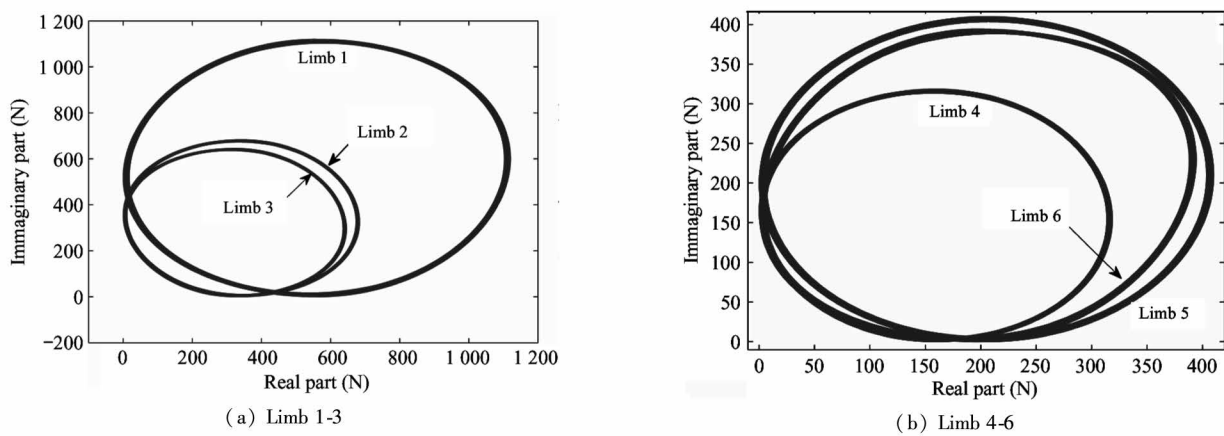


Fig. 5 Axial force of six limbs in complex plane

4 Experimental validation

4.1 Experimental design

Prototype is manufactured as presented in Fig. 6 together with the test site. It is necessary to declare that no case of 6 dimensional vibration occurs simultaneously in practical environment. Objective of the experiment is to verify the correctness of mobility matrix modeling strategy based on the axial force solution. Table 2 shows the arrangement of hammer and accelerators correspondingly.

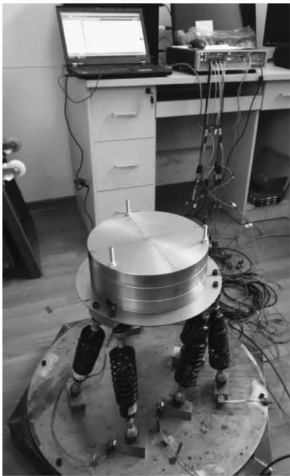
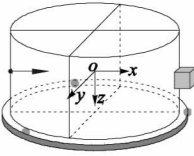
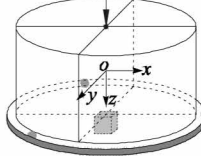
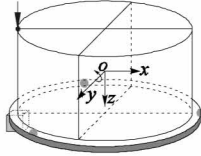


Fig. 6 Prototype of multi-DIM isolator and experimental setup

Table 2 Arrangement for hammer and accelerator of multi-DIM isolator experiment

| Testing dimension | Along x -axis | Along z -axis | About y -axis |
|-------------------|---|---|--|
| Arrangement |  |  |  |

Symbol annotation:  accelerator,  position and direction of hammer.

The force and the acceleration along x - and z -axis can be measured directly. The moment and the angular acceleration about y -axis could be calculated by combining with the measured signals as

$$\mathbf{M}_y = \mathbf{F}r_A \quad (40)$$

$$\alpha_y = \mathbf{a}/r_U \quad (41)$$

where, \mathbf{M}_y and α_y are moments and angular accelera-

tions, r_A and r_U are the radius of rigid body source and the distribution circle of spherical pairs B_1 - B_3 in up platform. Mobility power flowing into the isolator can be calculated by cross power spectra density G_{Fa} . Force (moment) and (angular) acceleration signals at upper end of each limb can be converted according to Table 3.

Table 3 Conversion coefficients list of generalized signals at upper end of each limb

| Coordinate axes | Limb 1 | Limb 2 | Limb 3 | Limb 4 | Limb 5 | Limb 6 |
|-----------------|---------|---------|---------|----------|----------|----------|
| y | $M_y/2$ | $M_y/8$ | $M_y/8$ | $M_y/12$ | $M_y/12$ | $M_y/12$ |

4.2 Experimental results

Mobility power flow composed of 3 independent vibrations along x -axis, along z -axis and about y -axis are shown in Fig. 7. It can be seen obviously that overall trend of the input and the transmitted power flows are extremely identical. The value of power flow decreases with the increase of frequency, which means that high frequency power flow component decreases.

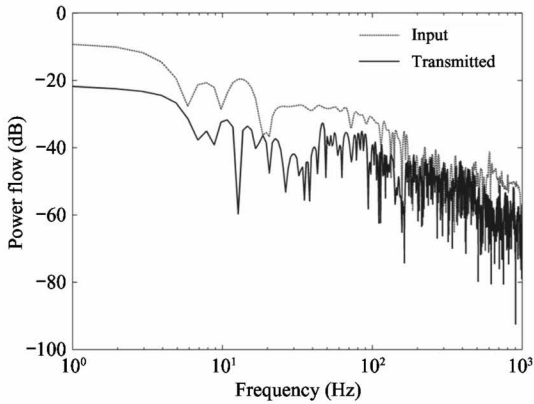


Fig. 7 Experimental power flow composed of 2T-1R vibration through multi-DIM isolator

Power flow transmissibility is plotted in Fig. 8. It can be found that both of experimental and numerical transmissibility are distributed perfectly flat, and trend of both transmissibility could be regarded almost as a constant in low frequency range (< 5 Hz). In middle

frequency range (6 – 92.4 Hz), deviation appears gradually. Numerical result exhibits a smooth as before, while the experimental result fluctuates remarkably, and the peaks begin to increase in quantity and intensity. It is noteworthy that more peaks appear and become obvious in higher frequency range (> 100 Hz) for both results. For whole investigated frequency range, two curves indicate a favorable consistency, which verifies the correctness and effectiveness of the mobility power flow model.

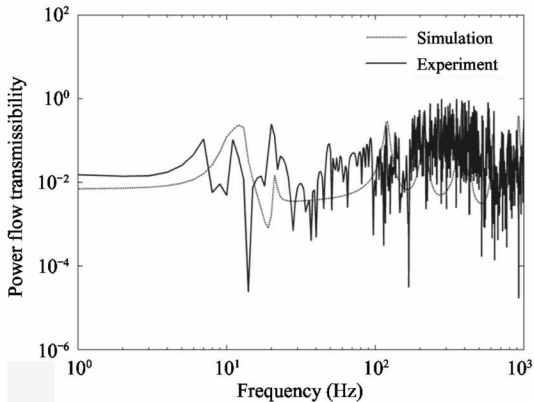


Fig. 8 Comparison between the simulation and the experimental power flow transmissibility

5 Conclusions

This paper proposes an axial force solution-based

mobility matrix modeling strategy for a weakly coupled parallel multi-DIM isolator. Mathematical model of mobility power flow is established via the mobility matrix and the transmissibility is simulated. Numerical results show that the response, including velocity and force, at bottom spherical joints would be influenced by the weak coupling of single opened chain. The comparison between the simulated and the experimental transmissibility shows meaningful differences. Trend of both transmissibility curves confirms well in low frequency range (<5 Hz). In middle frequency range ($6-92.4$ Hz), deviation appears gradually. It is noteworthy that more peaks appear and intensity becomes more obvious in higher frequency range (>100 Hz) for both results. As a conclusion, axial force solution-based strategy is a good way to obtain the mobility matrix of the titled multi-DIM isolator.

References

- [1] Geng Z, Haynes L. Six degree-of-freedom active vibration control using the Stewart platforms [J]. *IEEE Transactions on Automatic Control*, 1994, 2(1): 45-53
- [2] Spanos J, Rahman Z, Blackwood G. A soft 6-axis active vibration isolator[C]//Proceedings of the American Control Conference, Washington, USA, 1995: 412-416
- [3] Liu C, Jing X, Daley S, et al. Recent advances in micro-vibration isolation[J]. *Mechanical Systems and Signal Processing*, 2015, 56(8): 55-80
- [4] Duan X, Qiu Y, Mi J. On the mechatronic servo bandwidth of a Stewart platform for active vibration isolating in a super antenna[J]. *Robotics and Computer-Integrated Manufacturing*, 2016, 40: 66-77
- [5] Wang C, Xie X, Chen Y. Investigation on active vibration isolation of a Stewart platform with piezoelectric actuators[J]. *Journal of Sound and Vibration*, 2016, 383: 1-19
- [6] Wu Y, Yu K, Jiao J. Dynamic modeling and robust nonlinear control of a six-DOF active micro-vibration isolation manipulator with parameter uncertainties[J]. *Mechanism and Machine Theory*, 2015, 92: 407-435
- [7] Cheng Y, Ren G, Dai S. The multi-body system modeling of the Gough-Stewart platform for vibration control[J]. *Journal of Sound and Vibration*, 2004, 271(3-5): 599-614
- [8] Joshi A, Kim W. Multivariable control for hexapod-based satellite vibration isolation[J]. *Journal of Dynamic Systems, Measurement, and Control*, 2005, 35(2): 129-134
- [9] Hanieh A. Active isolation and damping of vibrations via Stewart platform[D]. Belgium: Free University of Brussels (ULB), Active Structures Laboratory, 2003: 199-201
- [10] Cheng Y, Ren G, Dai S. Vibration control of Gough-Stewart platform on flexible suspension[J]. *IEEE Transactions on Automatic Control*, 2003, 19(3): 489-493
- [11] Ren G, Lu Q, Hu N, et al. On vibration control with Stewart parallel mechanism[J]. *Mechatronics*, 2014, 14(1): 1-13
- [12] Lu Y, Zhu W, Ren G. Feedback control of a cable-driven Gough-Stewart platform[J]. *IEEE Transactions on Automatic Control*, 2006, 22(1): 198-202
- [13] Mizuno T, Murashita M, Takasaki M, et al. Pneumatic three-axis vibration isolation system using negative stiffness[C]//Proceedings of the 44th IEEE Conference on Decision and Control, Seville, Spain, 2005: 12-15
- [14] Mizuno T, Yuji I, Masaya T. A three-axis vibration isolation system using modified zero-power controller with parallel mechanism technique[J]. *Mechatronics*, 2011, 21(6): 1055-1062
- [15] Yun Y, Li Y. Modeling and control analysis of a 3-PUPU dual compliant parallel manipulator for micro positioning and active vibration isolation[J]. *Journal of Dynamic Systems, Measurement, and Control*, 2012, 134(2): 1-9
- [16] Zhang Q, Jin J, Zhang J, et al. Active vibration suppression of a 3-DOF flexible parallel manipulator using efficient modal control[J]. *Shock and Vibration*, 2014, 2014(2): 107-129
- [17] Zhu W. Research on semi-active control of multi-DIM vibration absorber based on MR damper and parallel mechanism[D]. Zhenjiang: College of Mechanical Engineering, Jiangsu University, China, 2007: 49-62
- [18] Li D, Zhang J, Li W. Simulation of multi-DIM vibration reduction based on PKM weakly-coupling design[J]. *Journal of Machine Design*, 2014, 31(1): 20-26 (In Chinese)
- [19] Li D, Zhang J. Mobility matrix of a thin circular plate carrying concentrated masses based on transverse vibration solution[J]. *Shock and Vibration*, 2014, 2014(2): 1-15
- [20] Zhang J, Li D. Mobility power flows of thin circular plate carrying concentrated masses based on structural circumferential periodicity[J]. *Journal of Mechanical Engineering and Science*, 2016, 230(17): 2996-3011

Li Desheng, born in 1983. He received his Ph.D degree in Mechanical Engineering Department of Tianjin University in 2015. He also received his B.S. and M.S. degrees from Shandong Institute of Light Industry and Tianjin University of Technology in 2006 and 2009, respectively. His research interests include vibration & noise reduction and mechanical design.